A Hard X-Ray Scanning Microprobe for Fluorescence Imaging and Microdiffraction at the Advanced Photon Source*

Z. Cai, B. Lai, W. Yun[#], P. Ilinski, D. Legnini, J. Maser. and W. Rodrigues[%]

Experimental Facilities Division, Argonne National Laboratory, Argonne, IL 60439
[#] Advanced Light Source, LawrenceBerkeley National Laboratory, Berkeley, CA 94720
[%]Department of Physics & Astronomy, Northwestern University, Evanston, IL 60208

Abstract. A hard x-ray scanning microprobe based on zone plate optics and undulator radiation, in the energy region from 6 to 20 keV, has reached a focal spot size (FWHM) of 0.15 μm (v) x 0.6 μm (h), and a photon flux of $4x10^9$ photons/sec/0.01%BW. Using a slit 44 meters upstream to create a virtual source, a circular beam spot of 0.15 μm in diameter can be obtained with a photon flux of one order of magnitude less. During fluorescence mapping of trace elements in a single human ovarian cell, the microprobe exhibited an imaging sensitivity for Pt (L_α line) of 80 attograms/μm^2 for a count rate of 10 counts per second. The x-ray microprobe has been used to map crystallographic strain and multiquantum well thickness in micro-optoelectronic devices produced with the selective area growth technique.

The recent availability of high-brilliance synchrotron radiation sources[1] and x-ray Fresnel zone plate microfocusing optics with high spatial resolution and high focusing efficiency[2] has made possible the creation of a new tool for material characterization on micron and submicron length scales. A hard x-ray microprobe (HXRM) that combines microfocusing capabilities with x-ray sensitivity to trace element distributions, crystallographic strain, and the ability to penetrate deep in a specimen, has been developed for high-resolution fluorescence mapping and microdiffraction at the Advanced Photon Source (APS) at Argonne National Laboratory.

The HXRM utilizes the radiation from the high-brilliance source generated from an electron beam of 7 GeV in the APS storage ring and a 3.3-cm-period undulator (APS undulator A). The energy of the radiation can be tuned from 3.2 to 45 keV by a combination of varying the undulator gap and selecting among the first, third, and fifth harmonics of the undulator. The undulator has been optimized so that continuity in brilliance is achieved when tuning from one harmonic energy to the next.

The HXRM is installed in a dedicated beamline (2-ID-D) specifically designed and developed for x-ray microscopic applications. The beamline was specially designed to achieve conservation of the source brilliance, selectivity of energy bandwidth, and the capability of reducing the effective source size. The beamline uses a windowless operation between the front end and the beamline to avoid degradation of wavefront due

DISCLAIMER

DISCLAIMER

Portions of this document may be illegible in electronic image products. Images are produced from the best available original document.

to vacuum barriers. The nominal emittance of the beam in the APS storage ring is 8.2×10^{-9} m-rad. Given a one-percent coupling between the vertical and horizontal emittance and beta functions of 14 m in horizontal and 6 m in vertical, the FWHM source size of the photon beam at the center of the straight section is 52 μm in vertical and 790 μm in horizontal. In order to preserve the brilliance, we use a water-cooled grazing incidence (0.15°) horizontally deflecting mirror (1.2 meters long) as a first optical component. The grazing incidence of the mirror considerably reduces the power density on the reflecting surface and thus improves the performance of the first component. The cutoff of the reflected energy provided by the mirror considerably reduces both total radiation power and heat flux incident on downstream optical components, thus enhancing their performance. The horizontal deflection geometry takes advantage of less stringent requirements in slope error for avoiding brilliance degradation in the horizontal direction because the emittance in the horizontal direction is two orders of magnitude larger than that in vertical direction. Three reflecting surfaces (Si, Rh, and Pt) cover x-ray energies up to 40 keV. Use of the mirror also provides suppression of high-order harmonics of the undulator radiation, which is particularly important for high-energy storage rings like that of the APS. Either a double-crystal monochromator (DCM) or a double-multilayer monochromator (will be installed soon) located 64 to 65 meters from the source is used to monochromatize the mirror-reflected undulator beam. The combination of the large monochromator-to-source distance and the power filtering of the mirror reduces the maximum power density at normal incidence at the monochromator to less than 13.3 W/mm^2, thirteen times less than that of a beamline without mirror filtering and with the monochromator located in the first optical enclosure. When a proper mirror coating is used, the maximum heat flux on the first crystal is less than 2.3 W/mm^2. A monolithic, U-shaped, and water-cooled Si(111) crystal, with less than 2 microradians of tangential slope error over the footprint of the FWHM of the undulator radiation, is used as the first crystal for the DCM. It can handle a peak heat flux of 5W/mm^2 before the beam brilliance degradation becomes severe.

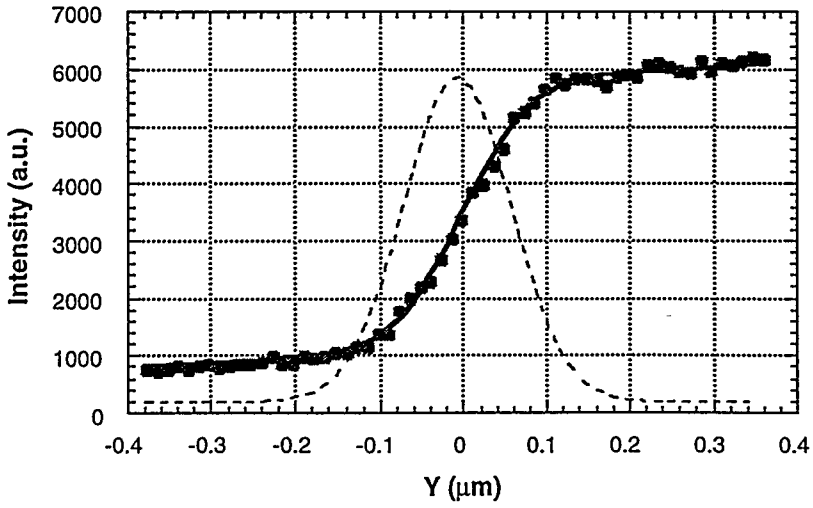

Fig 1. Resolution test of a zone plate at E = 8 keV using a Cr knife edge scan. Dots are measured fluorescence intensity, solid line is the fitting curve, and the dashed line is the derivative of the fitted curve. The FWHM beam size is measured to be 150 nm.

The phase zone plates we have developed for the HXRM have first-order focusing efficiency from 15% to 40% within the x-ray energy region from 6 keV to 20 keV.[3] The thickness of the gold zone plates ranges from 1.5 μm to 3.5 μm, and the focal length ranges from 5 cm to several meters at 8 keV. The outer most zone width, which determines the spatial resolution of the focusing optics, has reached 100 nm. Future development of the phase zone plates will improve the spatial resolution and extend the capability of the HXRM toward higher energy. In the meantime, x-ray energies higher than 20 keV can be achieved by employing a multiple-zone-plate stacking technique. The HXRM is located in the experiment station 71.5 meters away from the source. For a zone plate with a focal length of 10 cm at 8 keV and a diameter of 150 μm, we have a demagnification factor of 710. In order to coherently illuminate the zone plate in the horizontal direction so that a horizontal spot size limited by the outer most zone with of the zone plate is obtained, a water-cooled and adjustable slit located 28.3 meters from the center of the insertion device straight section is used to reduce the effective horizontal source size.

The vertical size of the focal spot generated from a zone plate of 10-cm focal length at 8 keV is shown in Fig. 1. The profile was obtained by scanning a 100-Å-thick Cr knife edge across the focal spot and measuring its fluorescence intensity. The FWHM spot size was obtained by first fitting the fluorescence intensity profile with error functions and then taking derivative of the fitted profile. Using a Si(111) monochromator, we have obtained a focal spot size (FWHM) of 0.15 μm (v) x 1.0 μm (h)[4] and a photon flux of $4x10^9$ photons/sec at the focal spot and thus a photon flux density gain of 15,000. A circular beam spot 0.15 μm in diameter can be achieved by creating a virtual source (horizontal only) at 43.5 meters upstream of the zone plate, with an order of magnitude less flux in the focal spot.

The HXRM consists of a zone plate, a platinum order-sorting aperture (5-30 μm) for selecting the first-order focused beam, and a sample holder assembly that allows three orthogonal translations and a full rotation around a vertical axis (theta rotation). The translation stages on the sample assembly provide a minimum step size of 0.1 μm. A peizo-driven XY stage on the assembly provides finer scanning steps. The sample assembly also contains chi and phi segments for angular positioning of samples when performing diffraction experiments. The HXRM is equipped with a Ge energy-dispersive detector (a 13-element detector will be installed soon) for fluorescence measurements and a CCD or NaI detector mounted on the 2-theta arm for diffraction measurement. In the following, we describe two experiments using the microprobe to demonstrate its capability.

Cisplatin is an anticancer agent that is currently used for the treatment of testicular, ovarian and other tumors. The effectiveness of the agent sometimes is limited because the cancer cells develop resistance to this drug. There have therefore been intensive efforts over the last decade to develop derivatives, which maintain anticancer activity against cisplatin-resistant cells. A group[5] in La Trobe University, Australia, has recently

identified a cisplatin derivative (Pt103) that has good activity against cisplatin-resistant cells in culture. In order to quantitatively determine the effectiveness of the Pt103 agent,

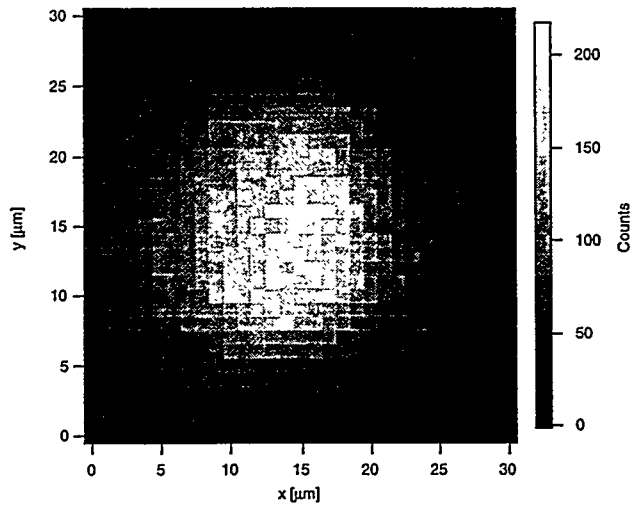

Fig. 2. X-ray fluorescence image of Pt distribution in an ovarian cancer cell treated with cisplatin. The specimen was provided by D. Phillips' group in La Trobe University, Australia.

x-ray fluorescence mapping of platinum's L_α-line emission has been used to image ovarian cancer cells with and without development of cisplatin resistance, at increasing times of exposure to cisplatin and Pt103, respectively. Figure 2 shows a platinum image of an ovarian tumor cell treated with cisplatin. The level of detection sensitivity of platinum is crucial in determining the concentration of platinum in cells that have developed resistance and been exposed to cisplatin for a short time. There is an overlap between the spectrum of the Pt-L_α line and the Cu-K_β, Zn-K_α and Zn-K_β lines. Both Cu and Zn are trace elements in the cell. Therefore, the platinum count rate at each pixel of the image in Fig. 2 was obtained through a careful fitting of the spectrum among the spectra of Cu, Zn, and Pt.[6] The microprobe exhibits sensitivity for the Pt-L_α line of 80 attograms/μm^2 with a count rate of 10 counts per second. Our results show that the x-ray microprobe detection of platinum in tumor cells is many orders of magnitude better than that of a proton microprobe, and the sensitivity now available is suitable for studies of platinum distribution in tumor cells subjected to clinical dose of platinum anticancer agents.

An electroabsorption modulator laser (EML) array for telecommunication requires sophisticated integration of multiquantum well (MQW) lasers, modulators, and optical waveguides on different regions of the same wafer. Integration is possible in the quaternary alloys $In_{1-x}Ga_xAs_{1-y}P_y$ because of the metal-organic-chemical-vapor deposition (MOCVD) technique of selective area growth (SAG). While the group III precursors in MOCVD readily bond to a free InGaAsP surface, they will not stick to a SiO_2 surface. Therefore, the group III precursors just above a thin oxide mask patterned onto the InGaAsP can then diffuse to the free-InGaAsP surface in the vicinity of the oxide, leading to an enhancement of the epitaxial growth rate. By the appropriate choice of an

oxide mask pattern, SAG allows precise control of the spatial variation of multilayer thickness, composition, and crystallographic strain on micron length scales. In order to understand the details of the growth process, we have measured the crystallographic

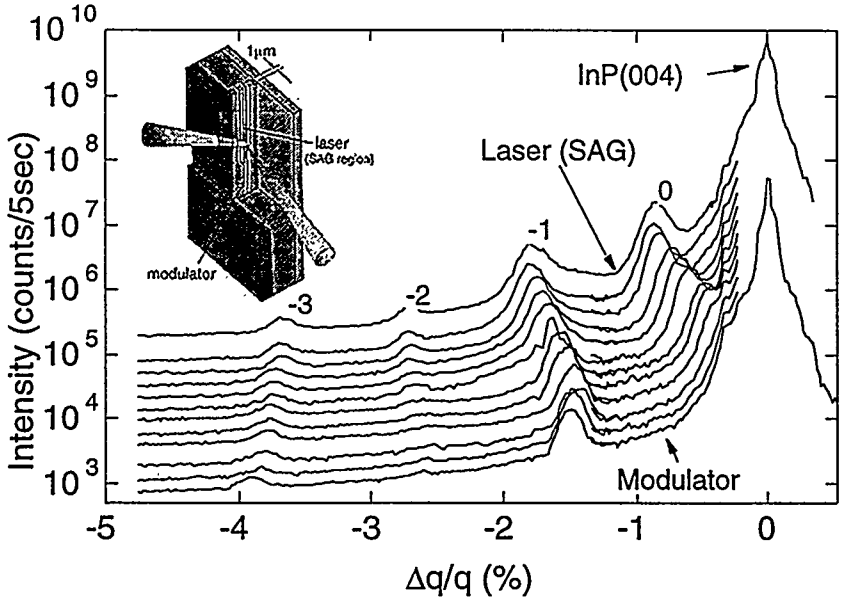

Fig. 3. X-ray microdiffraction along the multilayer growth direction in a fully processed EML device measured with a 0.5 μm x-ray spot. The position of the x-ray beam is scanned from the thickness-enhanced MQW laser region to the modulator region where there is no growth enhancement.

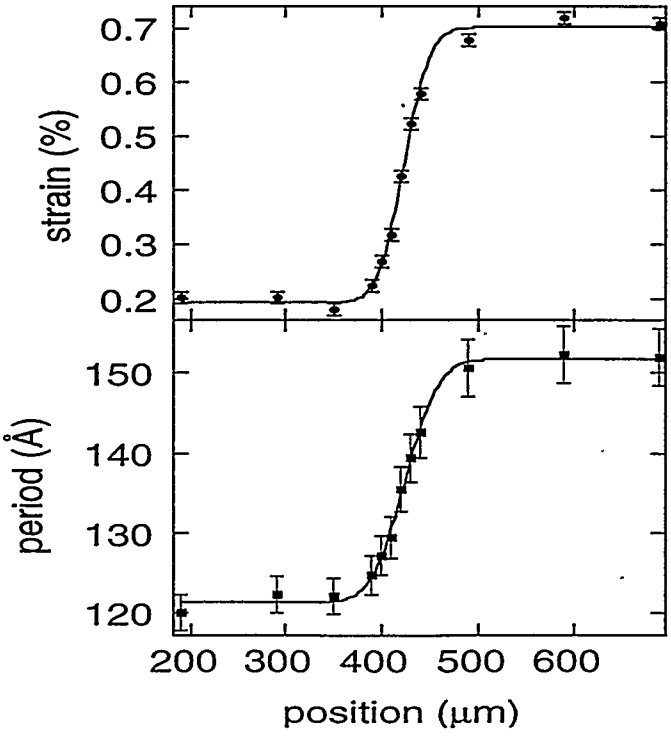

Fig. 4. MQW period and average perpendicular strain as a function of position.

strain and multilayer thickness of as-grown InGaAsP multilayer device material produced with SAG. The microprobe was needed because of the ultrasmall volume of material in the active region of optoelectronic device. Figure 3 shows a series of microdiffraction scans taken from an EML device with an active mesa of MQW about 1 μm wide (see the inset in Fig. 3). The principal features in Fig. 3 are the InP(004) substrate Bragg peak and the MQW superlattice peaks labeled by order. The position of the zero-order peak gives the average strain perpendicular to the layer of the MQW. The separation between the adjacent superlattice peaks is proportional to the inverse of the MQW period. In the Fig. 4, we plot the MQW period and average perpendicular strain, which clearly show that the MQW material varies smoothly from the laser to the modulator.

Since the commissioning of the HXRM in December 1997, the microprobe has been used for the development of many x-ray microfocusing-based techniques and a broad range of scientific applications. They include high-spatial-resolution fluorescence microscopy,[6-8] diffraction microscopy,[9-12] microspectroscopy,[7] fluorescence correlation spectroscopy,[13] and fluorescence tomography.[14] In addition, we are currently carrying out experiments of transmission microscopy and transmission microtomography.

*This work was supported by the Department of Energy, Basic Energy Sciences, Office of Science, under Contract No. W-31-109-ENG-38.

REFERENCES

1. G. K. Shenoy, P. J. Viccaro, and D. M. Mills, Argonne National Laboratory Report, ANL-88-9.
2. B. Lai, W. Yun, D. Legnini, Y. Xiao, J. Chrzas, P. Viccaro, V. White, S. Bajikar, D. Denton, F. Cerrina, E. Di Fabrizio, M. Gentili, L. Grella, and M. Baciocchi, *Appl. Phys. Lett.* **61**, 1877(1992).
3. W. Yun, B. Lai, A. Krasnoperova, E. Di Fabrizio, Z. Cai, F. Cerrina, Z. Chen, M. Gentili, E. Gluskin, *Rev. Sci. Instrum.* **70**, 3537 (1999).
4. W. Yun, B. Lai, Z. Cai, J. Maser, D. Legnini, E. Gluskin, Z. Chen, A. Krasnoperova, Y. Valdimirsky, F. Cerrina, E. Di Fabrizio, M. Gentili, *Rev. Sci. Instrum.* **70**, 2238 (1999).
5. D. Phillips et al., unpublished results.
6. P. Ilinski, B. Lai, Z. Cai, W. Yun, D. Legnini, T. Talarico, M. Cholewa, D. Phillips et al., to be submmited.
7. W. Yun, S. Pratt, R. Miller, Z. Cai, D. Hunter, A. Jarstfer, K. Kemner, B. Lai, H-R. Lee, D. Legnini, W. Rodrigues, C. Smith, *J. Synchrotron Rad.* **5**, 1390 (1998).
8. K. Kemner, W. Yun, Z. Cai, B. Lai, H-R. Lee, J. Maser, D. Legnini, W. Rodrigues, J. Jastrow, R. Miller, S. Pratt, M. Schneegurt, C. Kulpa Jr., *J. Synchrotron Rad.* **6**, 639 (1999).
9. Z. Cai, W. Rodrigues, P. Ilinski, D. Legnini, B. Lai, W. Yun, E. Isaacs, K. Lutterodt, J. Grenko, R. Glew, S. Sputz, J. Vandenberg, R. People, M. Alam, M. Hybertsen, L. Ketelsen, *Appl. Phys. Lett.* **75**, 100 (1999).
10. H. Solak, Y. Vladimirsky, F. Cerrina, B. Lai, W. Yun, Z. Cai, P. Ilinski, D. Legnini, W. Rodrigues, *J. Appl. Phys.* **86**, 884 (1999).
11. H.-R. Lee, D. Kupperman, W. Yun, Z. Cai, W. Rodrigues, *Rev. Sci. Instrum.* **70**, 175 (1999).
12. G. Wong, Y. Li, I. Koltover, C.R. Safinya, Z. Cai, W. Yun, *App. Phys. Lett.* **73**, 2042 (1998).
13. J. Wang, A.K. Sood, P.V. Satyam, Y. Feng, X. Wu, Z. Cai, W. Yun, S.K. Sinha, *Phys. Rev. Lett.* **80**, 1110 (1998).
14. M. Naghedolfeizi, J. –S. Chung, G. E. Ice, W. Yun, Z. Cai, B. Lai, *Mat. Res. Soc. Symp. Proc.* **524**, 233 (1998).